# Novel technique for the calculation of eddy current losses and Lorentz forces in foil winding transformers

Guillermo A. Díaz Flórez<sup>a,\*</sup>, Enrique E. Mombello<sup>b</sup> and Stephan Voss<sup>c</sup>

**Abstract.** This paper presents a new methodology to calculate eddy current losses and Lorentz forces in foil winding transformers. This methodology is based on the equivalent winding current distribution in the foil winding and the iron core obtained by means of the Semianalytic Integral Method (SAIM) [1]. The main advantage of the calculation technique presented in this paper is that it is based on mathematical expressions which are compact and easy to evaluate, thus achieving a considerable reduction in the overall time required to determine the design parameters of the transformer. The results obtained from the proposed formulation have been compared to those obtained using the finite element method (FEM) using as a case study a 10 MVA transformer and an excellent agreement between both techniques has been obtained.

Keywords: Integral methods, surface current, finite-element method (FEM), skin effect, proximity effect

## 1. Introduction

The precise calculation of transformer parameters is of great importance in the design stage for both rated and transient operating conditions. Among the most relevant parameters are the short circuit impedance [2,3], eddy current losses in the windings [4] and Lorentz forces in the windings in short circuit conditions [5].

There are several alternatives for the design of low voltage windings for high currents, for example, helical coils, layer windings made of arrangements of rectangular conductors connected in parallel and also windings made of continuously transposed conductor CTC [6]. In recent years the use of foil conductor has received great attention from manufacturers because of its large cross section, ease of manufacturing and its low cost compared to other conductors.

An adequate prediction of the spatial distribution of winding losses is of great importance, since it is the basis for the determination of hot spots that can produce dangerous temperatures in the interturn insulation. These temperatures can cause insulation damage and short circuits between turns, which will reduce the life of the transformer [7,8].

<sup>&</sup>lt;sup>a</sup>Universidad de La Salle, Bogota, Colombia

<sup>&</sup>lt;sup>b</sup>CONICET – Universidad Nacional de San Juan, San Juan, Argentina

<sup>&</sup>lt;sup>c</sup>Siemens A.G., Nürenberg, Deutschland

<sup>\*</sup>Corresponding author: Guillermo A. Díaz Flórez, Universidad de la Salle, Cra 2 # 10-70, Building C, 7th floor, Bogota, Colombia. Tel.: +571 3535360; E-mail: guandiaz@unisalle.edu.co.

As is well known, foil windings are usually used for inner windings, thereby the prediction of the spatial distribution of Lorentz forces enables the calculation of mechanical stresses and allows taking measures to avoid permanent deformations of these coils due to short circuits, such as buckling [9].

In the case of external windings, the spatial distribution of Lorentz forces determines the maximum radial stresses in the conductors, making it possible their proper sizing to prevent stresses which could permanently deform them [10].

One of the particular aspects of transformers designed with foil windings is that there is a very sensitive trade-off between the accuracy of the calculation and the simulation time [1,4]. If sufficiently reliable results are required, numerical methods such as the finite element method (FEM) should be used, which require rather long calculation times for this type of transformers [11].

On the other hand, if quick results are required, analytical methods can be used at the risk of sacrificing the accuracy of the solution [12]. The problem of the trade-off between accuracy and computational speed has been addressed in [1], where a hybrid approach between analytical and numerical techniques is proposed, providing results in a very short calculation time and keeping the accuracy required for transformer design purposes.

Reference [1] presents the methodology for determining the surface current distribution for the equivalent models of the core and windings of the transformer. The present article deals in detail with the formulation required to determine the power losses and the Lorentz forces in the foil winding from the solution of the current surface distribution of each element of the equivalent transformer model obtained by means of the Semianalytic Integral Method.

Since the formulations presented here are an application of the Semianalytic Integral Method, the details that may be necessary to fully understand them can be found in [1].

#### 2. Proposed model

This section describes the conventions related to mathematical notation, physical laws and gives a description of the equivalent magnetic model of the transformer to be used.

#### 2.1. Lorentz forces

Lorentz equation states that if a surface current density  $\vec{K}$  is subjected to the magnetic field intensity  $\vec{H}$ , then it will experience an electrodynamic force  $\vec{F}$  according to Eq. (1)

$$\vec{F} = F_r \hat{r} + F_z \hat{z} = \mu_0 \int_{S'} \vec{K} \times \vec{H} ds'$$
 (1)

where  $\mu_0$  is the magnetic permeability of vacuum and S' the surface along which the current density  $\vec{K}$  flows. It should be noted that the magnitudes in Eq. (1) are instantaneous values, and further expressions are required to consider the sinusoidal nature of the vector fields. Additionally, since both the magnetic field strength and the surface current density are assumed to be sinusoidal, the cross product between them yields a Lorentz force having a unidirectional component  $\vec{F}^{(DC)}$  and also a double frequency sinusoidal component  $\vec{F}^{(AC)}$ . The corresponding equations are given below

$$\underline{\vec{F}}^{(AC)} = \frac{\mu_0}{2} \int_{S'} \underline{\vec{K}} \times \underline{\vec{H}} \, \mathrm{ds'}$$
 (2)

$$\vec{F}^{(DC)} = \frac{\mu_0}{2} \int_{S'} \text{Re}\left(\underline{\vec{K}} \times \underline{\vec{H}}^*\right) ds'$$
 (3)

Once the values of both components have been obtained, the forces in the time domain can be determined as follows

$$F_r(t) = F_r^{(DC)} + \left| \underline{F}_r^{(AC)} \right| \cdot \cos \left[ 2\omega t + \arg \left( \underline{F}_r^{(AC)} \right) \right]$$
(4)

$$F_{z}(t) = F_{z}^{(DC)} + \left| \underline{F}_{z}^{(AC)} \right| \cdot \cos \left[ 2\omega t + \arg \left( \underline{F}_{z}^{(AC)} \right) \right]$$
 (5)

where  $\omega = 2\pi f$  is the rated angular frequency.

## 2.2. Power losses

The power losses in a conductor are

$$P = \frac{1}{2\sigma} \int_{\mathbf{V}'} \vec{\underline{J}} \cdot \vec{\underline{J}}^* d\mathbf{v}'$$
 (6)

where  $\sigma$  is the material conductivity and  $\vec{J}$  is the current density [13]. Furthermore, the thin-sheet approximation allows modeling solid conductors by means of surface current distributions insofar as its thickness d is much less than the penetration depth  $\delta$  of the magnetic field, and this condition is met for foil conductor coils. The thin-sheet approximation states that

$$\underline{\vec{J}} = \frac{1}{d}\underline{\vec{K}} \tag{7}$$

The substitution of Eq. (7) into Eq. (6) yields

$$P = \frac{1}{2\sigma d^2} \int_{\mathbf{V}'} \underline{\vec{K}} \cdot \underline{\vec{K}}^* d\mathbf{v}'$$
 (8)

A detailed description of the thin-sheet approximation can be found in [14].

#### 2.3. Equivalent magnetic model of the transformer

An equivalent magnetic model of the transformer based on an arrangement of surface current elements is proposed in [1]. This arrangement can be seen in Fig. 1.

As shown in Fig. 1, the yokes of the core have been represented by disk shaped elements, while the elements belonging to the leg of the core and the windings have been represented by cylindrical elements. The thickness of all elements of the model is infinitesimal. It should be noted that each element has an x in its central part, which represents a field evaluation point. Each field point has an associated index, which is the index of the element to which it belongs, so that the field point  $P_{ax}^{[j]}$  is located in the central part of the j-th element.

The transformer model has a total amount of n elements, of which  $m=m_c+m_{ef}$  initially have unknown current densities. The core has been modeled using  $m_c$  elements while the foil winding using  $m_{ef}$  elements. The methodology for determining the current densities of the m elements associated with the core and the foil conductor winding has been presented in [1] in detail, so that it will be assumed that the current densities of the equivalent model elements have been previously calculated. In particular, the current density of the elements belonging to the foil conductor winding is

$$\underline{\vec{K}}^{[j]} = \underline{K}_{\phi}^{[j]} \hat{\phi} \tag{9}$$

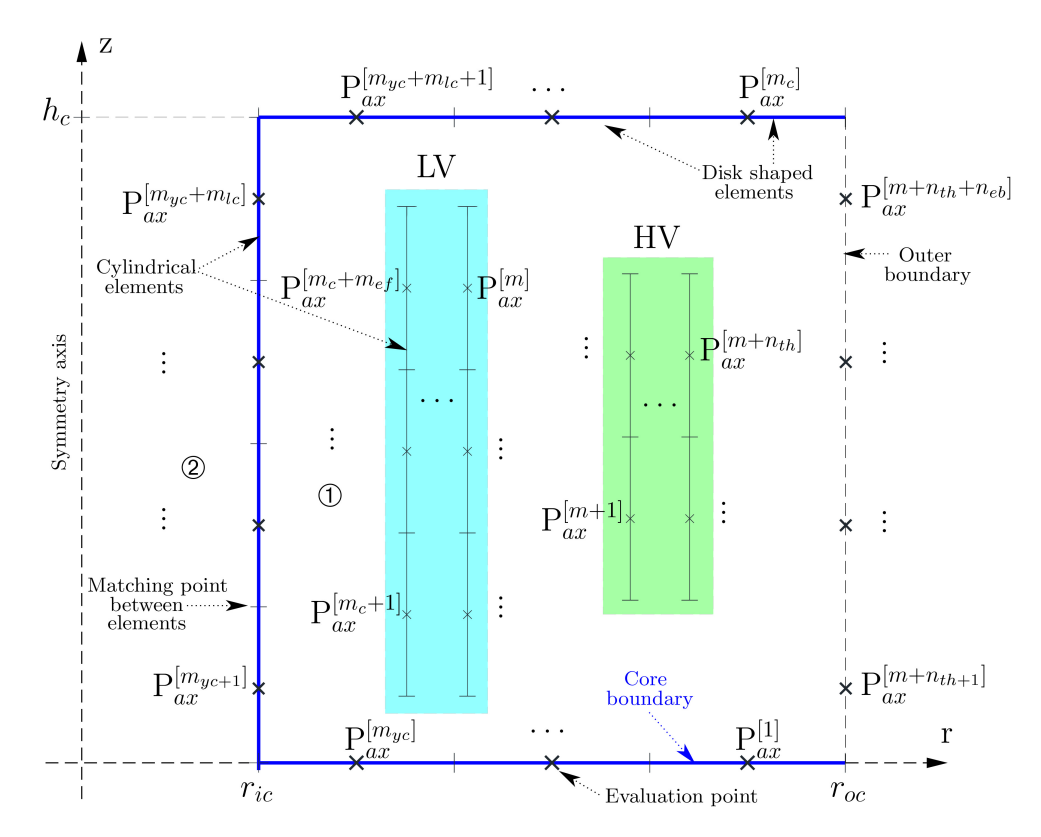


Fig. 1. Axisymmetric equivalent magnetic model of the transformer.

where  $j = m_c + 1 \cdots m$ ,  $\underline{K}_{\phi}^{[j]}$  is the surface current density distribution of the j-th element and  $\hat{\phi}$  is the unit vector in the azimuthal direction.

Another characteristic of SAIM is that the current density is assumed to vary linearly between the ends of the elements, that is

$$\underline{K}_{\phi}^{[j]} = \frac{\underline{K}_{\phi 2}^{[j]} - \underline{K}_{\phi 1}^{[j]}}{z_{2}^{[j]} - z_{1}^{[j]}} \left( z' - z_{1}^{[j]} \right) + \underline{K}_{\phi 1}^{[j]}$$
(10)

where  $\underline{K}_{\phi 1}^{[j]}$  and  $\underline{K}_{\phi 2}^{[j]}$  are the current densities at the bottom and the top of the cylindrical element respectively. Additionally, z' is the axial coordinate of an arbitrary point on the surface of the cylindrical element so that  $z_1^{[j]} \leqslant z' \leqslant z_2^{[j]}$ , where  $z_1^{[j]}$  is the axial coordinate of the bottom end and  $z_2^{[j]}$  is the axial coordinate of the top end of the j-th element. It should be noted that the current densities  $\underline{K}_{\phi 1}^{[j]}$  and  $\underline{K}_{\phi 2}^{[j]}$  of all elements are assumed to be known.

The reason for choosing a linear current distribution is because this choice has shown a reasonable balance between the complexity of the mathematical expressions and the accuracy in solving the whole transformer model. Although it is theoretically possible to model the field produced by higher order elements (i.e. quadratic or cubic), these choices considerably increase the complexity of the analytical mathematical expressions of the elements [1].

#### 3. Solution methodology

This section presents the methodology to determine the magnetic field strength in each field point of the equivalent transformer model. The mathematical expressions to determine the power losses and Lorentz forces in the foil conductor winding will be introduced later.

## 3.1. Magnetic field strength calculation at the evaluation points

It is evident from Eq. (1) that in addition to the surface current distribution  $\vec{K}$  it is also necessary to know the distribution of the magnetic field strength  $\vec{H}$  in order to determine Lorentz forces. As mentioned, the surface current distribution is known, however it is necessary to propose an efficient methodology to calculate the magnetic field strength at the points of interest. According to the above, this section will be dedicated to derive the necessary formulation to determine the magnetic field strength at the selected field points of the equivalent transformer model.

The equivalent transformer model of Fig. 1 defines  $s=m+n_{th}+n_{eb}$  field points, of which  $n_{th}$  field points have been placed in the high voltage winding, while  $n_{eb}$  field points are located on the outer boundary of the model. According to [1] and the equations proposed in [15–17], it is possible to determine the interaction matrices which contain the geometry dependent factors. These geometry dependent factors represent the magnetic effect (geometric part) of each element on each field point. The structure of these matrices is presented below

$$\mathbf{k}_{r}^{(\aleph)} = \begin{bmatrix} k_{r1}^{[1,1]} & k_{r2}^{[1,1]} & \cdots & k_{r1}^{[1,n]} & k_{r2}^{[1,n]} \\ \vdots & \vdots & \ddots & \vdots & \vdots \\ k_{r1}^{[s,1]} & k_{r2}^{[s,1]} & \cdots & k_{r1}^{[s,n]} & k_{r2}^{[s,n]} \end{bmatrix}_{s \times 2n}$$
(11)

$$\mathbf{k}_{z}^{(\aleph)} = \begin{bmatrix} k_{z1}^{[1,1]} & k_{z2}^{[1,1]} & \cdots & k_{z1}^{[1,n]} & k_{z2}^{[1,n]} \\ \vdots & \vdots & \ddots & \vdots & \vdots \\ k_{z1}^{[s,1]} & k_{z2}^{[s,1]} & \cdots & k_{z1}^{[s,n]} & k_{z2}^{[s,n]} \end{bmatrix}_{s \times 2n}$$
(12)

Each of the rows of these matrices is associated with a field point, while the columns are associated with field sources. Note also that there are two columns for each element, because there are two geometry dependent factors per element, since the field strength produced by the i-th element on the j-th field point is

$$\vec{H}^{[j,i]} = H_r^{[j,i]} \hat{r} + H_z^{[j,i]} \hat{z}$$
(13)

where

$$\begin{split} \underline{H}_{r}^{[j,i]} &= k_{r1}^{[j,i]} \underline{K}_{\phi 1}^{[i]} + k_{r2}^{[j,i]} \underline{K}_{\phi 2}^{[i]} \\ \underline{H}_{z}^{[j,i]} &= k_{z1}^{[j,i]} \underline{K}_{\phi 1}^{[i]} + k_{z2}^{[j,i]} \underline{K}_{\phi 2}^{[i]} \end{split}$$

for  $i=1\cdots n$  and  $j=1\cdots s$ . More details on the definition of the geometry dependent factors can be found in [1]. A vector containing all surface current densities of the model can be defined as follows:

$$\underline{\mathbf{K}}_{\phi}^{(\aleph)} = \begin{bmatrix} \underline{\mathbf{K}}_{\phi}^{(uk)} \\ \underline{\mathbf{K}}_{\phi}^{(kn)} \end{bmatrix}_{2n \times 1}.$$
(14)

where  $\underline{\mathbf{K}}_{\phi}^{(uk)}$  is a subvector with the current densities of the elements belonging to the core and the foil conductor winding, while  $\underline{\mathbf{K}}_{\phi}^{(kn)}$  contains the current densities of the high voltage winding. Note that  $\underline{\mathbf{K}}_{\phi}^{(\aleph)}$  is a column vector of 2n rows because each element is characterized by two values of surface current density. The magnetic field strength at each field point can be determined directly by means of the following matrix products

$$\underline{\mathbf{H}}_{r}^{(\aleph)} = \mathbf{k}_{r}^{(\aleph)} \cdot \underline{\mathbf{K}}_{\phi}^{(\aleph)} \tag{15}$$

$$\underline{\mathbf{H}}_{z}^{(\aleph)} = \mathbf{k}_{z}^{(\aleph)} \cdot \underline{\mathbf{K}}_{\phi}^{(\aleph)} \tag{16}$$

where  $\underline{\mathbf{H}}_r^{(\aleph)}$  and  $\underline{\mathbf{H}}_z^{(\aleph)}$  are column vectors of s rows with the following structure

$$\underline{\mathbf{H}}_{r}^{(\aleph)} = \begin{bmatrix} \underline{H}_{r}^{[1]} \\ \vdots \\ \underline{H}_{r}^{[j]} \end{bmatrix}_{s \times 1}, \underline{\mathbf{H}}_{z}^{(\aleph)} = \begin{bmatrix} \underline{H}_{z}^{[1]} \\ \vdots \\ \underline{H}_{z}^{[j]} \\ \vdots \\ \underline{H}_{z}^{[s]} \end{bmatrix}_{s \times 1}.$$

$$(17)$$

where  $\underline{H}_r^{[j]}$  and  $\underline{H}_z^{[j]}$  are the magnetic field strengths components in radial and axial direction due to the contributions of all elements at the field point j,  $j=1\cdots s$ . According to the above, the magnetic field strength at the field point j can be written as

$$\vec{\boldsymbol{H}}^{[j]} = H_r^{[j]} \hat{\boldsymbol{r}} + H_z^{[j]} \hat{\boldsymbol{z}} \tag{18}$$

Expanding the intensity of radial and axial field in its real and imaginary parts, the above expression can be rewritten as follows:

$$\underline{\vec{H}}^{[j]} = \left(H_r^{(\text{Re})[j]} + \mathbf{j} \cdot H_r^{(\text{Im})[j]}\right)\hat{r} + \left(H_z^{(\text{Re})[j]} + \mathbf{j} \cdot H_z^{(\text{Im})[j]}\right)\hat{z}. \tag{19}$$

where j is the imaginary unit and the superscripts (Re) and (Im) denote the real and imaginary part respectively. It should be noted that it is also possible to determine the magnetic field strength at each field point by superimposing the individual contributions of each of the elements, however, this method turns out to be inefficient and generally it is not recommended when n and s are large.

On the other hand, the calculation by matrix product as proposed in Eqs (15) and (16) is very efficient computationally, insofar as specialized tools like Matlab, Octave, Scilab or libraries as Lapack are used, since these tools use optimized routines to reduce the computational complexity of matrix products compared to the calculation term by term. Furthermore, these specialized routines currently provide support for multithreaded processing, which further increases the evaluation speed.

#### 3.2. Expressions for calculating Lorentz forces in the foil conductor winding

As shown in Fig. 1, the equivalent model of the foil conductor winding is an arrangement of cylindrical elements of infinitesimal thickness. Since this arrangement is magnetically equivalent to solid conductor turns [1], Lorentz forces acting on these elements are also equivalent to the forces that would act on the real winding of solid conductors. To determine Lorentz forces on the elements belonging to the foil

conductor winding, the definitions in Eqs (2) and (3) will be used. The differential surface in cylindrical coordinates is  $ds' = r'd\phi'dz'$ . Using the surface integrals explicitly for an arbitrary cylindrical element indexed as j, the following expressions are obtained

$$\underline{\vec{F}}^{(AC)[j]} = \frac{\mu_0 r'^{[j]}}{2} \int_{z_1^{[j]}}^{z_2^{[j]}} \int_0^{2\pi} \underline{\vec{K}}^{[j]} \times \underline{\vec{H}}^{[j]} d\phi' dz', \tag{20}$$

$$\vec{\mathbf{F}}^{(DC)[j]} = \frac{\mu_0 r'^{[j]}}{2} \int_{z_1^{[j]}}^{z_2^{[j]}} \int_0^{2\pi} \operatorname{Re}\left(\underline{\vec{\mathbf{K}}}^{[j]} \times \underline{\vec{\mathbf{H}}}^{[j]*}\right) d\phi' dz'$$
(21)

where  $j = m_c + 1 \cdots m$ . The term  $r'^{[j]}$  corresponds to the radius of the element j, i.e., the average radius of the foil conductor turn [1]. It should be noted that  $r'^{[j]}$  does not depend on  $\phi'$  or z', that is why it has been extracted from the integral. Lorentz forces can be written in vector form as follows,

$$\vec{\underline{F}}^{(AC)[j]} = F_x^{(AC)[j]} \hat{r} + F_z^{(AC)[j]} \hat{z}$$
(22)

$$\vec{F}^{(DC)[j]} = F_r^{(DC)[j]} \hat{r} + F_z^{(DC)[j]} \hat{z}$$
(23)

where,

$$\underline{F}_r^{(AC)[j]} = F_r^{(AC_{Re})[j]} + j \cdot F_r^{(AC_{Im})[j]}$$
(24)

$$E_z^{(AC)[j]} = F_z^{(AC_{Re})[j]} + j \cdot F_z^{(AC_{Im})[j]}$$
(25)

Substituting the generic expressions of  $\underline{\vec{K}}^{[j]}$  and  $\underline{\vec{H}}^{[j]}$  (Eqs (9) and (19) respectively) into Eqs (20) and (21), and after performing the vector product and the analytical integration with respect to  $\phi'$  and z', the following solutions for the AC double frequency components are obtained

$$F_r^{(AC_{Re})[j]} = -\frac{\mu_0 \pi}{2} r'^{[j]} (z_2^{[j]} - z_1^{[j]})$$
 (26)

$$\left\{ H_z^{(\text{Im})[j]} \left( K_{\phi 1}^{(\text{Im})[j]} + K_{\phi 2}^{(\text{Im})[j]} \right) - H_z^{(\text{Re})[j]} \left( K_{\phi 1}^{(\text{Re})[j]} + K_{\phi 2}^{(\text{Re})[j]} \right) \right\}$$

$$F_r^{(AC_{\text{Im}})[j]} = \frac{\mu_0 \pi}{2} r'^{[j]} (z_2^{[j]} - z_1^{[j]})$$
(27)

$$\left\{ H_z^{(\text{Re})[j]} \left( K_{\phi 1}^{(\text{Im})[j]} + K_{\phi 2}^{(\text{Im})[j]} \right) + H_z^{(\text{Im})[j]} \left( K_{\phi 1}^{(\text{Re})[j]} + K_{\phi 2}^{(\text{Re})[j]} \right) \right\}$$

$$F_z^{(AC_{Re})[j]} = \frac{\mu_0 \pi}{2} r'^{[j]} (z_2^{[j]} - z_1^{[j]})$$
 (28)

$$\left\{ H_r^{(\text{Im})[j]} \left( K_{\phi 1}^{(\text{Im})[j]} + K_{\phi 2}^{(\text{Im})[j]} \right) - H_r^{(\text{Re})[j]} \left( K_{\phi 1}^{(\text{Re})[j]} + K_{\phi 2}^{(\text{Re})[j]} \right) \right\}$$

$$F_z^{(AC_{Im})[j]} = -\frac{\mu_0 \pi}{2} r'^{[j]} (z_2^{[j]} - z_1^{[j]})$$
 (29)

$$\left\{ H_r^{(\text{Re})[j]} \left( K_{\phi 1}^{(\text{Im})[j]} + K_{\phi 2}^{(\text{Im})[j]} \right) + H_r^{(\text{Im})[j]} \left( K_{\phi 1}^{(\text{Re})[j]} + K_{\phi 2}^{(\text{Re})[j]} \right) \right\}$$

The corresponding equations for the unidirectional components (DC) are as follows

$$F_r^{(DC)[j]} = \frac{\mu_0 \pi}{2} r'^{[j]} (z_2^{[j]} - z_1^{[j]}) \cdot \left\{ H_z^{(Im)[j]} \left( K_{\phi_1}^{(Im)[j]} + K_{\phi_2}^{(Im)[j]} \right) + H_z^{(Re)[j]} \left( K_{\phi_1}^{(Re)[j]} + K_{\phi_2}^{(Re)[j]} \right) \right\}$$
(30)

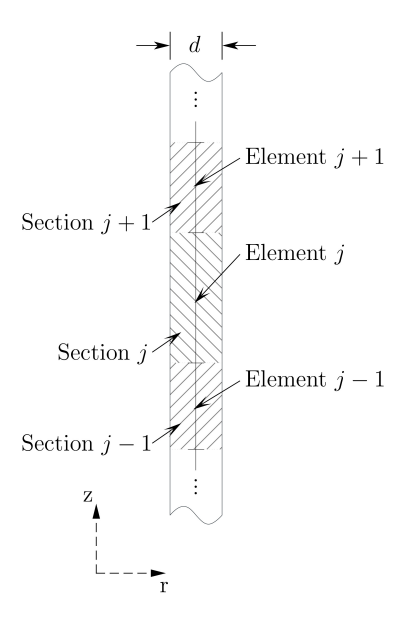


Fig. 2. Segmentation of the foil conductor turn.

$$F_z^{(DC)[j]} = -\frac{\mu_0 \pi}{2} r'^{[j]} (z_2^{[j]} - z_1^{[j]}) \cdot \left\{ H_r^{(Im)[j]} \left( K_{\phi_1}^{(Im)[j]} + K_{\phi_2}^{(Im)[j]} \right) + H_r^{(Re)[j]} \left( K_{\phi_1}^{(Re)[j]} + K_{\phi_2}^{(Re)[j]} \right) \right\}$$
(31)

The total forces acting on the whole foil conductor winding can be determined by means of the following expressions

$$\vec{F}^{(DCf)} = \sum_{j=m_c+1}^{m} \vec{F}^{(DC)[j]}$$
(32)

$$\underline{\vec{F}}^{(ACf)} = \sum_{j=m_c+1}^{m} \underline{\vec{F}}^{(AC)[j]}$$
(33)

Once the DC and double frequency AC Lorentz force components have been calculated, it is possible to determine the forces on each element as a function of time using Eqs (4) and (5).

#### 3.3. Expressions for the power losses in the foil conductor winding

Equation (8) is used to determine the power losses of the winding. Because the current density in the foil conductor winding has significant variations along the axial dimension, a subdivision of each coil in axial sections as shown in Fig. 2 is proposed. It can be seen that the sections have been defined so that the coordinates of the bottom and top ends of each element match the coordinates of adjacent elements.

Similarly, an index is defined for each section, so that it also matches the index of the respective element. According to the above, and considering the integral of Eq. (8) explicitly for an arbitrary section j, the following expression is obtained.

$$P^{[j]} = \frac{1}{2\sigma d^2} \int_{z_1^{[j]}}^{z_2^{[j]}} \int_0^{2\pi} \int_{r_1^{[j]}}^{r_2^{[j]}} r' \left( \underline{\vec{K}}^{[j]} \cdot \underline{\vec{K}}^{[j]*} \right) dr' d\phi' dz', \tag{34}$$

Substituting Eq. (10) into Eq. (9) and then  $\underline{\vec{K}}^{[j]}$  into Eq. (34), performing the scalar product, integrating analytically and evaluating at the limits of integration, the following expression is obtained for the power losses of the j-th turn section

$$P^{[j]} = \frac{\pi \left( z_2^{[j]} - z_1^{[j]} \right) \left( r_2^{[j]2} - r_1^{[j]2} \right)}{6d^2 \sigma} \cdot \begin{pmatrix} K_{\phi 1}^{(\text{Re})[j]2} + K_{\phi 1}^{(\text{Im})[j]2} + K_{\phi 2}^{(\text{Re})[j]2} + K_{\phi 2}^{(\text{Im})[j]2} + K_{\phi 2}^{(\text{Im}$$

where  $r_1^{[j]}$  and  $r_2^{[j]}$  are the inner and outer radii of the j-th turn segment respectively. Therefore, the total power losses of the whole foil conductor winding, termed  $P^{(f)}$ , is given as the superposition of the effects of all its segments, so that

$$P^{(f)} = \sum_{j=m_c+1}^{m} P^{[j]} \tag{36}$$

#### 4. Results and validation

### 4.1. Description of the case study

In order to validate the formulations proposed in this work, the calculation of Lorentz forces and power losses of a 10 MVA transformer with a foil conductor low voltage winding and a high-voltage winding made of several layers of paper-insulated solid rectangular conductor has been performed. The detailed construction data of the case study transformer, the amount of elements used to model the core, the foil conductor winding and the high voltage winding can be found in Table 1 of [1]. The methodology proposed in [1] has been used to obtain the current distribution of each element, which is necessary for the calculation of power losses and Lorentz forces. The radial and axial components of the magnetic field strength of each field point has been determined using Eqs (15) and (16).

#### 4.2. Lorentz forces

From the surface current densities of each element and the magnetic field strength of each field point, the components of Lorentz forces have been computed using Eq. (26) through Eq. (31). Then, they have been transformed into the time domain by Eqs (4) and (5). Because the Lorentz force varies both spatially and temporally, a specific time was selected to calculate the force. The selected time was t=8.33 ms, time at which the double frequency component of the Lorentz force has its maximum. To calculate the forces it was assumed that the peak value of the phase current of the windings is equal to the peak value of the asymmetric short-circuit current which was determined as described in [18] from the reactive and resistive short circuit impedance values of the case study transformer.

Figure 3 shows the distribution of axial Lorentz forces. As it can be seen, the representation has been done as force density, i.e., force per unit area N/m<sup>2</sup>. In this case the surface is the cross section of the specific turn section being analyzed (see Fig. 2). The reason for this is that the magnitude and direction of the force vary according to the analyzed turn sector. Figure 3 shows significant variations of the force at coil ends.

The distribution of axial forces of Fig. 3 shows that the contribution of the central part of the winding is practically zero, while compressive forces exist at the ends of the turns closest to the core leg, i.e., there are forces in the  $+\hat{z}$  direction at the bottom end, and forces in the  $-\hat{z}$  direction at the top end.

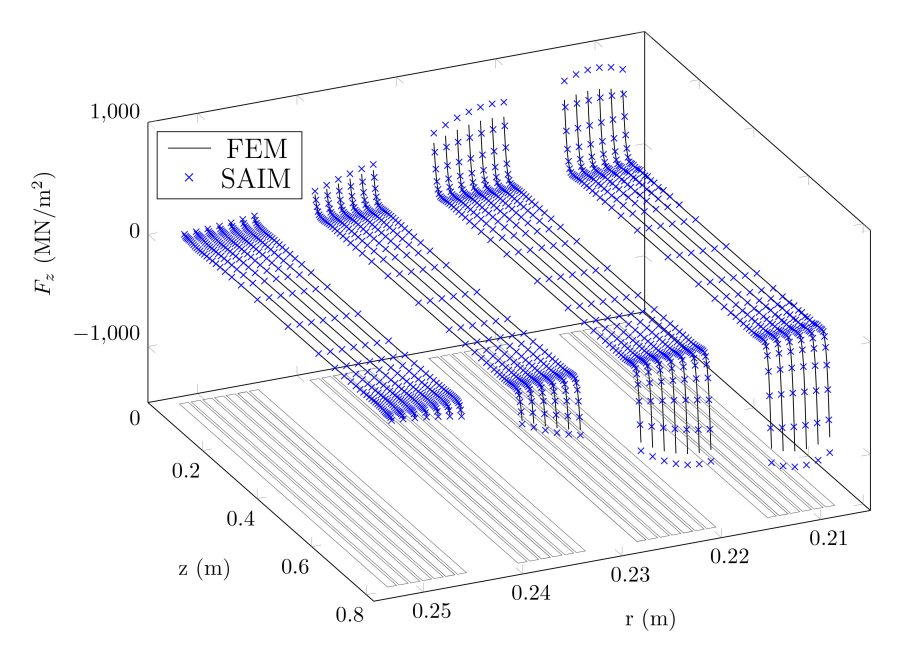


Fig. 3. Spatial distribution of axial Lorentz forces in the foil conductor winding.

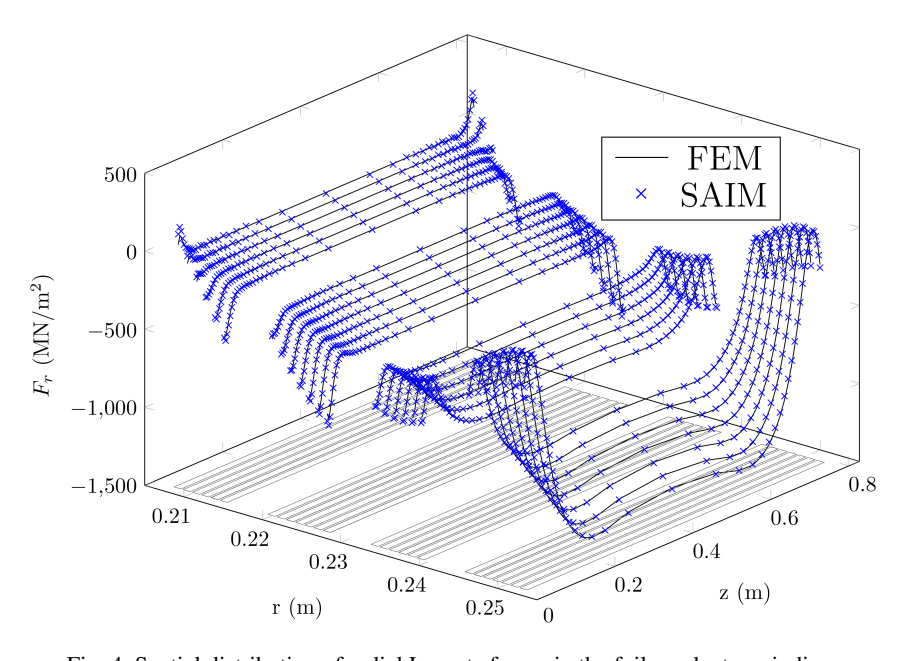


Fig. 4. Spatial distribution of radial Lorentz forces in the foil conductor winding.

This is due to the important radial field component at the first winding turns. Figure 4 depicts the spatial distribution of radial forces in the foil conductor winding.

The forces are predominantly compressive  $(-\hat{r}$  direction). The maximum radial force contribution is located in the middle of the turns nearest to the leakage duct (duct between windings), however it should be noted that the maximum cumulative force occurs in the first coils closer to the core due to the

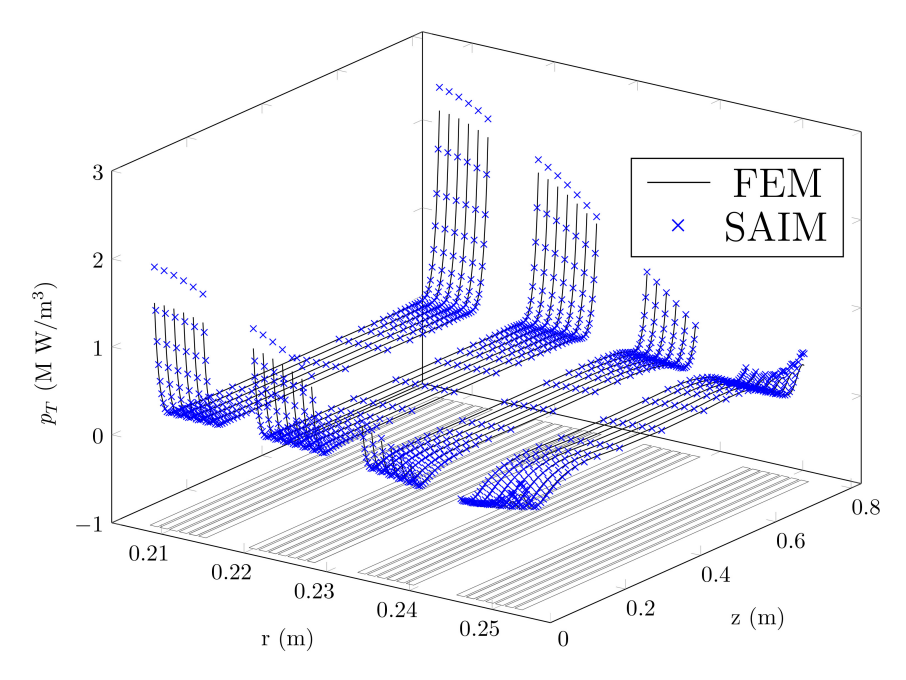


Fig. 5. Power loss density in the foil conductor winding.

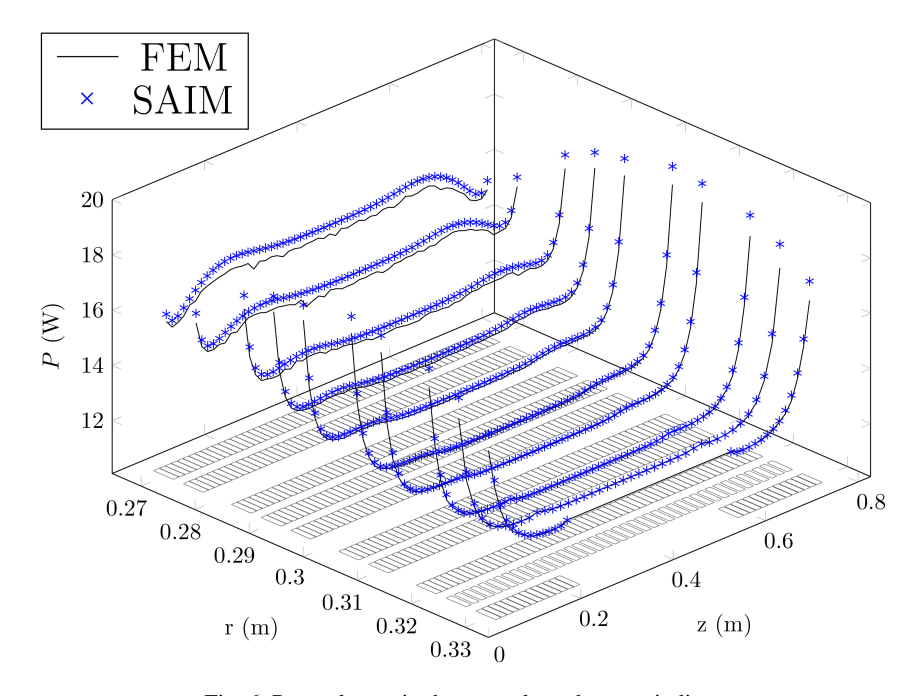


Fig. 6. Power losses in the normal conductor winding.

superposition of the interactions from the other turns of the winding. It can also be seen in Fig. 4 that the forces at the ends of the turns closest to the leakage duct are very small compared to the ones at the center.

Table 1 Summary of total power losses of the windings

Method	$P^{(f)}(W)$	$P^{(h)}\left(\mathbf{W}\right)$
FEM	6 118.2	7 083.7
SAIM	6 141.0	7 172.1

Table 2
Relation of calculation times reported by FEM and SAIM

Parameter	FEM	SAIM	Ratio FEM/SAIM
Total number of elements	112 827	1 370	82.36
Const. Discrt. Assemb. Solv. Eq. (s)	112.17	10.05	11.16
Calculation of par. of interest (s)	67.94	5.30	12.82
Total t. (s)	180.11	15.35	11.74

Table 3 Comparison between short-circuit forces computed with FEM and SAIM for  $t=8.33~\mathrm{ms}$ 

Element description	FEM F <sub>z</sub> (kN)	FEM $F_r$ (kN)	SAIM F <sub>z</sub> (kN)	SAIM $F_r$ (kN)	Rel. Err. $F_z$ (%)	Rel. Err. $F_r$ (%)
1st Turn LV	-2.360	-3.299	-2.373	-3.310	0.57	0.35
6th Turn LV	-2.074	-60.834	-2.086	-60.750	0.57	-0.14
11th Turn LV	-1.430	-122.292	-1.439	-121.960	0.66	-0.27
16th Turn LV	-0.726	-188.675	-0.732	-188.243	0.84	-0.23
21th Turn LV	-0.206	-264.559	-0.208	-265.655	0.87	0.41
26th Turn LV	-0.088	-354.937	-0.089	-354.177	0.63	-0.21
1st Layer HV	-1.653	937.728	-1.663	938.328	0.65	0.06
4th Layer HV	-3.134	677.181	-3.158	679.991	0.78	0.42
7th Layer HV	-4.504	374.405	-4.537	375.180	0.72	0.21
10th Layer HV	-5.672	25.258	-5.706	25.317	0.60	0.24

A comparison between the numerical values of radial and axial forces computed with FEM and SAIM is presented in the Table 3. Notice in Table 3 that *1st Turn LV* is the closest turn to the core, whereas the *1st Layer HV* is the closest layer to the main oil duct. The relative errors for  $F_z$  and  $F_r$  are reported in last two columns of Table 3 showing an excellent agreement between FEM and SAIM.

#### 4.3. Power losses

From the current density distribution of the surface current elements it is possible to determine the power losses at each section of a given turn by applying Eq. (35). Similarly to the case of Lorentz forces calculation, it is more appropriate to represent the power losses in the form of volume density in W/m<sup>3</sup>. In this case, the power losses of each section has been divided by its volume. Figure 5 shows the spatial distribution of power losses in the foil conductor winding.

There is a significant increase of the loss density at the turn ends nearest to the core yokes (in the order of 2 MW/m³), which could represent overheating points due to high concentration of losses. Furthermore, foil conductor windings are built on a Transformerboard formwork, so there is no adequate oil flow for these coils which are closest to the core, and this can be inconvenient for cooling these critical points.

Table 1 summarizes the results of total losses in the high and low voltage windings obtained using the proposed formulation compared with a simulation using the finite element method FEM. Details about the simulation using finite element based software Infolytica Magnet are presented in [1]. There

is an excellent agreement between the values of total power losses of the windings calculated using the proposed formulation (SAIM) and the ones obtained using FEM.

Because the magnetic field strength at each field point is available, it is easy to determine the additional losses factor for each turn of high voltage winding according to the formulations proposed in [6,10]. Figure 6 shows the calculation results of power losses in watts for each of the turns of the high voltage winding. It should be noted that the maximum loss value is located at coil ends of the most central layers, since the radial magnetic flux is high in this region, having a normal incidence to the conductors which increases the additional losses. An excellent agreement between the results of FEM and SAIM can be appreciated.

#### 4.4. Calculation times used by FEM and SAIM

Table 2 presents a relation of the computational performances of FEM (using Infolytica Magnet) and SAIM. As shown in the first row, FEM required nearly 80 times more elements than SAIM. The second row of the table presents the computing time needed for geometry construction, discretization, assembling and solving the equation system. The third row shows the time used on finding the parameters of interest (Lorentz forces and Losses), and the last row presents the total simulation time. The details related with the FEM simulation using Magnet can be found in [1].

#### 5. Conclusion

A new and fast methodology for the determination of power losses and Lorentz forces in transformers with foil conductor windings have been presented in this paper. The authors have developed new mathematical expressions for this purpose on the basis of the Semianalytic Integral Method (SAIM), which are compact and numerically easy to evaluate, thereby increasing the overall performance of SAIM.

A real transformer was used as case study to validate the methodology. The results obtained by applying the proposed methodology were compared with those obtained using FEM, whereupon an excellent agreement has been achieved.

The inclusion of the proposed expressions has extended SAIM to the calculation of Lorentz forces, which is an important improvement, as this contribution now allows SAIM to calculate the spatial distribution of both power losses and Lorentz forces in all elements in reduced computation times, which enhances the overall efficiency in the process of optimizing the design of foil winding transformers.

As a corollary, the application of SAIM to foil windings has revealed results that are consistent with those found in the literature [19] in the sense that this kind of winding gives rise to axial forces which are much lower in magnitude than the radial ones.

#### References

- [1] G. Diaz and E. Mombello, Semianalytic integral method for fast solution of current distribution in foil winding transformers, *Magnetics, IEEE Transactions on* **51** (Sept 2015), 1–9.
- [2] J. Wang, C. Jing, Y. Fan, L. Liu, Y. Du, J. Zhang, C. Jiao and Z. Cheng, Numerical simulation of 3d stray field and short circuit impedance for a phase-shifting rectifier transformer, *International Journal of Applied Electromagnetics and Mechanics* 33 (2010), 191–196.
- [3] E. Sorrentino and J.C. Burgos, Application of 2d linear modeling for computing zero-sequence short-circuit impedances of 3-phase core-type {YNynd} transformers, *Electric Power Systems Research* **122** (2015), 1–9.

- [4] M.T. Villen, J. Letosa, A. Nogués and R. Murillo, Procedure to accelerate calculations of additional losses in transformer foil windings, *Electric Power Systems Research* **95** (2013), 85–89.
- [5] H.-M. Ahn, S.-Y. Kim, J.-K. Kim, Y.-H. Oh and S.-C. Hahn, Numerical investigation for transient electromagnetic force computation of power transformer during short-circuit condition, *International Journal of Applied Electromagnetics and Mechanics* (2016), 1–9.
- [6] S.V. Kulkarni and S. Khaparde, Transformer engineering: design and practice. CRC Press, 2004.
- [7] S. Taheri, A. Gholami, I. Fofana and H. Taheri, Modeling and simulation of transformer loading capability and hot spot temperature under harmonic conditions, *Electric Power Systems Research* **86** (2012), 68–75.
- [8] M. Lee, H.A. Abdullah, J.C. Jofriet and D. Patel, Temperature distribution in foil winding for ventilated dry-type power transformers, *Electric Power Systems Research* **80**(9) (2010), 1065–1073.
- [9] A. Bakshi and S.V. Kulkarni, Analysis of buckling strength of inner windings in transformers under radial short-circuit forces, *IEEE Transactions on Power Delivery* **29** (Feb 2014), 241–245.
- [10] R.M. Del Vecchio, B. Poulin, P.T. Feghali, D.M. Shah and R. Ahuja, Transformer design principles: with applications to core-form power transformers. CRC Press, 2010.
- [11] B. Ram, Loss and current distribution in foil windings of transformers, *IEE Proceedings on Generation, Transmission and Distribution* **145** (Nov 1998), 709–716.
- [12] V. Zúbek, Eddy current losses in transformer low voltage foil coils, *Journal of Electrical Engineering* **56**(3–4) (2005), 95–99.
- [13] P. Solin, I. Dolezel, P. Karban and B. Ulrych, Integral methods in low-frequency electromagnetics. John Wiley & Sons, 2009.
- [14] H.E. Knoepfel, Magnetic fields: a comprehensive theoretical treatise for practical use. John Wiley & Sons, 2008.
- [15] G. Diaz and E. Mombello, New compact and singularity free formulations for the magnetic field produced by a finite cylinder considering linearly varying current density, *International Journal of Applied Electromagnetics and Mechanics* **50**(2) (2016), 483–501.
- [16] G. Díaz and E. Mombello, Magnetic field due to a finite current carrying disk considering a vari able current density along its radial dimension, *International Journal of Applied Electromagnetics and Mechanics* **42**(1) (2013), 119–136.
- [17] G. Díaz, E. Mombello and V. Stephan, Magnetic vector potential and magnetic field intensity due to a finite current carrying cylinder considering a variable current density along its axial dimension, *International Journal of Applied Electromagnetics and Mechanics* **40**(2) (2012), 133–147.
- [18] I. Standard, 60076-5. power transformers: Part 5 ability to withstand short circuit, *International Electrotechnical Commission (IEC)*, 2006.
- [19] G. Bertagnolli, Short-circuit duty of power transformers. ABB, 2013.